Nanosecond laser silicon micromachining

Jun Ren[*a], Sergei S. Orlov[a], and Lambertus Hesselink[a]
Helen Howard[b] and Alan Conneely[b]
[a]SSPL, CISX, Department of Electrical Engineering, Stanford University, Stanford, CA 94305, USA
[b]National Center for Laser Applications, NUI, Galway, Ireland

ABSTRACT

We present theoretical calculations and experimental measurements of silicon micromachining rates, efficiency of laser pulse utilization, and morphology changes under UV nanosecond pulses with intensities ranging from 0.5 GW/cm^2 to 150 GW/cm^2. Three distinct irradiance regimes are identified based on laser intensity. At low intensity, proper gas dynamics and ablation vapor plume kinetics are taken into account in our theoretical modeling. At medium high intensity, we incorporate the proper plasma dynamics, and predict the effects of the laser generated vapor plasma and the electron hole plasma on the laser-matter interaction. At even higher intensity, we attribute the observed increased ablation rate to energy re-radiation from the laser heated hot plasma, the strong shock wave, and the accompanied strong shock wave heating effects. Experimentally measured data in these regimes agree well with our calculations, without changing parameters in the calculations used for the three regimes. Our results can be applied toward quantitatively characterize the behavior of ablation results under different laser parameters to achieve optimal results for micromachining of slots and vias on silicon wafers.

Keywords: nanosecond, laser ablation, silicon, thermal evaporation, plasma, shock wave, metastable liquid

1. INTRODUCTION

Silicon, due to its abundance on earth and its wide applications in the electronics industry has become the mostly studied semiconductor element. Laser processing of silicon using nanosecond UV laser pulses with its high precision and fast processing time provides an important alternative to silicon micro machining. In principle, any type of nanosecond laser with laser intensities above the ablation threshold could potentially be utilized as a light source for silicon machining; and there are many nanosecond lasers available, with repetition rates varying from a few 10 kHz to a few Hz, with a maximum average per pulse intensity from a few GW/cm^2 to up to thousands of GW/cm^2, and a pulse length from a few nanoseconds to a few tens of nanoseconds. Experimental works[1,2] of UV laser ablation of metal Cu, Al, and metal alloy TiAl6V4 show scattered data in terms of ablation rate vs. the pulse intensity and pulse length, indicating non-linear dependences of the ablation rate on pulse intensity and pulse length. Hence, the efficiency of laser pulse utilization in terms of removing material is an important aspect that needs to be known before choosing laser sources. In this work, to our knowledge for the first time, we systematically calculate the ablation rate of silicon over a wide range of laser intensities ranging from 0.5 GW/cm^2 to 150 GW/cm^2 using nanosecond pulses of different pulse lengths. Our computational modeling provides estimations that can be quantitatively compared with experiments, and provides guidance how to best utilize the laser energy in the manufacturing processes, in order to have well characterized and well behaved machining results. Through our theoretical and experimental work, we discovered that as laser intensity increases, the laser silicon interaction could be divided into three distinct regimes based on laser intensity; namely, the low ablation intensity regime, the medium high intensity regime and the high intensity regime. Different ablation characteristics occur as results of different physical processes which dominate in these regimes. We include the comprehensive yet computationally treatable physical models and explanations in this work, and demonstrate good correspondence between our theoretical calculations and experimental verifications.

At low laser irradiance, even though the one dimensional heat flow equation[3,4] has been used to obtain satisfactory estimates of the liquid-solid position compared to experimental results[5,6], it doesn't include the vapor plume gas dynamics necessary to calculate the vapor phase front propagation, which is more relevant to the material removal rate from the surface by the laser pulses. Another possible approach is to use the Hertz-Knudsen equation in characterizing

[*] Electronic mail: junren@stanford.edu. Phone: (650)-723-4940

Photon Processing in Microelectronics and Photonics III, edited by P. R. Herman, J. Fieret, A. Piqué, T. Okada, F. G. Bachmann, W. Hoving, K. Washio, X. Xu, J. J. Dubowski, D. B. Geohegan, F. Träger, Proc. of SPIE Vol. 5339 (SPIE, Bellingham, WA, 2004) · 0277-786X/04/$15 · doi: 10.1117/12.529442

the vaporization flux[7], yet reasonable correspondences between theoretical estimations and experimental data for the silicon removal speed at the low irradiance regime would require the magnitudes of the saturated vapor pressure to be at least one order larger than the critical pressure, which is hard to explain with reliable physics. In our theoretical treatment of laser matter interaction at the low irradiance regime, we find good agreement between calculations and experimental verifications by using a one dimensional equilibrium vaporization theory developed by Anisimov (1968)[8,9]. The steady state surface receding speed and the re-condensation of the supersaturated vapor plume are characterized from the vapor gas dynamics. We apply the vaporization theory to the heat conduction equations and calculate the silicon removal rate under different nanosecond pulse lengths in the low irradiance regime.

As laser pulse energy increases into the medium irradiance regime, the laser generated plasma plays an important role in screening and re-distribution of laser energy during the ablation. Although many research works have been published to characterize the behavior of the plasma[10-14], little information is provided to quantitatively calculate the effects of the plasma on preventing the coupling between the incident laser beam and the ablating material. Here, we compute the behavior of the plasma, using proper plasma dynamics[15-17, 34-36], and characterize the effects of the vapor plasma above the surface and the electron-hole plasma in the bulk on the laser ablation of silicon. We apply the plasma modeling to the thermal equations, and good consistencies are found between our theoretical estimations and experimental data for different nanosecond pulse lengths at medium irradiance.

For laser silicon ablation at the very high intensity regime, limited information has been published in terms of ablation rate, ablation morphologies, and the mechanical properties of the ablation generated craters. A sudden drastic increase in ablation volume has been observed before[18,19] at laser intensities above 2.2×10^{10} W/cm^2 using 3ns, 266nm laser pulses and this increase in ablation volume was attributed to the transformation of nontransparent liquid metal into a transparent liquid dielectric at the critical state. In our work, we also experimentally observed increases in ablation speed both in the vertical and transverse directions using 5ns, 355nm laser pulses at very high laser intensities. However, from the previous discussions on strong plasma shielding effects at medium high laser intensities, it seems to make more sense to assume that at higher laser intensities, the plasma shielding effects would be stronger, which allows less interaction between the incident laser beam and the substrate. Furthermore, considering the experimental observations[18-20] that the majority of mass removal takes place a long time after the pulse; we think there should exist a secondary heating source that complements the primary laser pulse ablation and allows continuous energy exchange after the laser pulse. We attribute the observed increased ablation rate in the vertical direction to the energy re-radiation from the laser heated hot plasma. We calculate the energy accumulated in the plasma during the laser pulse, and apply the results to the phase explosion theory developed by Martynyuk (1974)[21]. In the transverse direction, we attribute the increased ablation rate to the increased plasma dimensions in the lateral direction and the strong shock wave with the strong shock heating effects[16]. Our approaches yield good agreement with the experimental results.

To investigate the laser ablation phenomena and correctly predict the outcomes for practical applications such as choosing the most proper nanosecond laser parameters for the specific silicon micromachining purposes, our approach is to set up an integrated picture that identifies the major dominating physical processes involved in each regime, to incorporate known physical phenomena into our modeling, and to specify and develop the descriptions of the dynamics of each interaction process. By doing so, we hope the interactions and inter-relations among these processes are fully accounted for, which is important for providing accurate estimation results through computational modeling.

2. NANOSECOND LASER SILICON REMOVAL UNDER VARIOUS IRRADIANCE REGIMES

The physical process of laser silicon interaction in the nanosecond time regime is a complex process, involving many aspects of laser matter interaction. As a laser beam with intensity above the ablation threshold illuminates the surface, the heat waves penetrate into the bulk of the silicon generating vapor and melt. Also, the surface plasma is formed by the incident laser beam. The surface plasma absorbs and reflects laser energy, and shock wave loading on surface is created primarily by the expansion of the plasma[23]. Cracks and fractures might appear as result of the large shock wave pressure and thermal stress. We divide the laser silicon interaction based on laser intensity into three distinct regimes; the low intensity regime, the medium high intensity regime and the high intensity regime. The major physical processes dominating in these three regimes include the nonlinear physical processes between the laser light and the condensed matter, the physical processes within the ablation generated vapor plume, and the physical processes between the laser ionized vapor plume and the ablating condensed matter. In the following sections, we will present both the

theoretical results and experimental verifications on how the laser silicon removal rate, ablation morphology and the efficiency of the laser pulse utilization change under nanosecond UV laser pulses with laser intensities ranging from 0.5 GW/cm^2 to 150 GW/cm^2.

2.1 Laser Silicon Interaction at the Low Ablation Intensity Regime

For silicon nanosecond UV laser ablation at low ablation intensity, the removal process takes place mainly through thermal surface vaporization. In our theoretical treatment at this regime, we find good agreement between calculations and experimental verifications by using a one-dimensional equilibrium vaporization theory developed by Anisimov (1968)[8,9]. In this model, based on the strong shock wave model[24,25], a discontinuity layer called the Knudsen layer is proposed in the hydrodynamic treatment of the vapor expansion[8,9]. Using an equilibrium approximation that the distribution function within the Knudsen layer is the sum of the distribution functions below and above the Knudsen layer with coordinate-dependent coefficients, steady state solutions for the surface receding speed and other parameters in vapor dynamics can be obtained by integration of the distribution function with considerations taken for the energy balance requirement. The surface receding speed $V_z|_{z=0}$ is therefore given by[8],

$$V_z|_{z=0} = \frac{(1-R)\times I}{\rho(H_v + 2.2k_B T(0)/M)} \qquad \text{(Eq.-1)}$$

Here I is the laser intensity, R is the surface reflection, and ρ is silicon density. H_v is the latent heat for vaporization. T(0) is the surface temperature and M is the atomic weight of silicon atoms. To solve for T(0), we substitute (Eq.-1) into the one dimensional self-sufficient heat transportation equations, (assuming laser spot size is much larger than the heat affected zone, $(\kappa\tau)^{1/2}$, κ is heat conductivity and τ is the laser pulse length),

$$\begin{aligned}
&C_p(z,t)\rho\frac{\partial T}{\partial t} = \nabla(\kappa(z,t)\nabla T) + C_p(z,t)\rho V_z|_{z=0}\ \Delta Q + S(z,t)\\
&S(z,t) = (1-R)\times\frac{I_0(t)}{\alpha(t)}e^{-z/\alpha(t)}\\
&\Delta Q|_{z\neq 0} = 0\\
&\Delta Q|_{z=0} = \rho H_v V_z|_{z=0} \qquad \text{(Eq.-2)}\\
&T(z,0) = 300K, T(\infty,t) = 300K
\end{aligned}$$

I(t) in our calculation is assumed to be of rectangular shape. Heat capacity C_p, density ρ, heat conductivity κ and optical absorption coefficient α are temperature dependent[3, 26,27]; their values will vary during the laser pulse,

$$\begin{aligned}
&\kappa(W/cm/K) = \begin{cases} 1.585T - 1.23 & T < 1370K \\ 0.221 & T > 1370K \end{cases}\\
&\alpha(1/cm) = \begin{cases} 1\times 10^6 e^{T/4545} & T \le 1100K \\ 1.27\times 10^6 & T > 1100K \end{cases}\\
&C_p = 0.814\ \text{J/g/K (solid)}, C_p = 0.914\ \text{J/g/K (liquid)}\\
&\rho = 2.3\ \text{g/cm}^3\ \text{(solid)}, \rho = 2.5\ \text{g/cm}^3\ \text{(liquid)}
\end{aligned} \qquad \text{(Eq.-3)}$$

Solving (Eq.-2), we could obtain the temperature distribution in the bulk of silicon and the steady state surface receding speed $V_z|_{z=0}$. The silicon removal speed defined as um per pulse is an integration of $V_z|_{z=0}$ over time,

$$d \approx \int_{t_0}^{\tau} (1-\delta) \times V_z \,|_{z=0}\, dt \qquad \text{(Eq.-4)}$$

Here t_0 is the start time for the integration; it is the larger value between the time needed for the surface temperature to reach 80% of its final value T(0) and the time needed for (Eq.-2) to settle to its stabilized state. δ is the degree of condensation introduced by the recondensation of the expanding vapor[8].

In our experiment, a high quality 355nm laser beam from Coherent AVIA laser system with $M^2 < 1.3$ is focused on a silicon sample surface using UV lens systems. The pulse length varies from 15.4ns to 22.6ns with intensity variations from around 0.5 GW/cm^2 to 4 GW/cm^2. The translation stage and thin film tester determine the focus positions and spot sizes[37]. After firing laser pulses on the silicon sample with a certain number of pulses, the ablated crater (blind hole) is measured using a Profilometer. The experimental measurements of the ablation removal speeds (um/pulse) are characterized as the averaged depth of the crater divided by the number of pulses applied. The number of applied pulses is changed from one to several tens. Good linear relationships between the applied number of pulses and the averaged depth of the craters are found when the aspect ratio is less than 4. (To exclude the removal contribution from melt flowing out of the generated crater, the applied pulse number at a slow ablation rate was set so that the generated craters were deep enough to be able to neglect the melt propelling part. The calculation and characterization of melt flow was based on a hydrodynamic fluid model[28].) In the case of ablation through the silicon sample, the removal speeds are given as the averaged removal volume per pulse divided by the area of the laser spot. Figure 1 shows the comparison of experimental measurements (hollow circles) and theoretical estimations (solid lines) of ablation removal speeds of silicon under 355nm laser pulses at low ablation laser intensity with laser pulse lengths of 15.4ns, 20ns and 22ns, respectively. Agreement can be found between our theoretical estimations and experimental measurements. Comparisons of experimental measurements and our physical modeling for the silicon removal rate at low ablation intensities are also carried out using shorter pulses, (a Quantum Ray laser system with 355nm wavelength and a 5ns pulse length is utilized as the ablation beam). We find good consistencies there as well.

As indicated in Figure 1, for laser intensities just above the ablation threshold, which is estimated using (Eq.-2) and (Eq.-4) as ~ 1×10^8 W/cm^2 for 20ns pulses, and ~ 3.5×10^8 W/cm^2 for 5ns pulses; the silicon removal rate undergoes fast increases with laser intensity. As laser intensity keeps increasing, after a certain point, the slope of the ablation rate vs. the laser intensity slows down. To characterize the dependence of the ablation rate on laser intensity, a parameter called the efficiency of laser pulse utilization η is introduced, where[22],

$$\eta = \frac{(H_v + H_m + C\times(T_b - T_0))\rho}{(1-R)\times I\times\tau}\times d \qquad \text{(Eq. -5)}$$

Figure 2 shows the calculated efficiency of laser pulse utilization as a function of the laser intensity for two pulse lengths. As shown, the efficiency of laser pulse utilization is about 10% to 15% better at longer pulses. The optimal intensities at which laser energies are best coupled into ablating the material are found to be slightly below 1 GW/cm^2 for 20ns pulses and above 1.5 GW/cm^2 for 5ns pulses. For both pulse lengths, the efficiency of utilizing the laser energy drops 30% to 40% from its peak as laser intensity increases above 3 GW/cm^2. Hence, in practical applications, where the pulse intensity and pulse repetition rate are inversely proportional to each other, it appears to be beneficial in terms of removing more material without increasing the total energy to choose the longer pulse length and the laser intensity where the best efficiency of laser pulse utilization is achieved.

Further comparisons of the morphologies of the ablation generated feature, including degree of debris and particulate accumulated around the perimeters show that ablation morphology is cleaner at shorter pulses. Also, in our morphology studies around the ablation site, we often tend to find many micro sized spherical droplets spreading around our sample, indicating to some extent the explosive boiling behavior. The explosive boiling behavior can be explained by the instability of the vaporization front generated by the subsurface superheating, where from our calculations of the temperature field distribution (and also from literature results[7,29]), it is indicated that the temperature reaches its maximum not on the surface but at some distance beneath the outer-most surface.

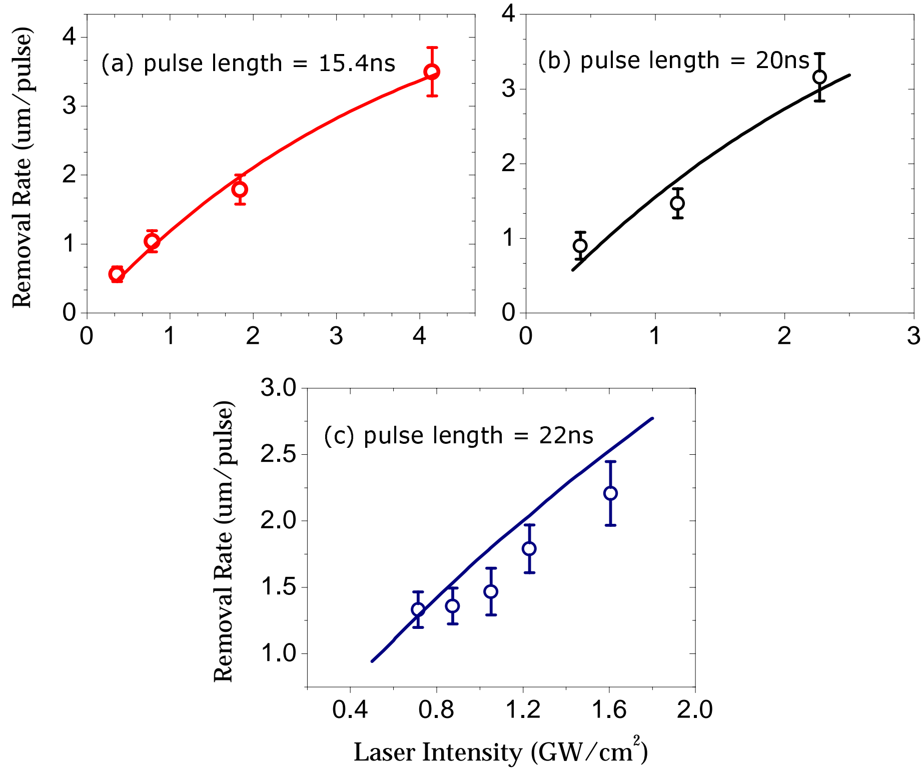

Figure 1: Comparison of experimental measurements (hollow circles) and theoretical estimations (solid lines) of ablation depth per pulse for 355nm pulses with pulse lengths of (a) 15.4 ns; (b) 20ns and (c) 22ns.

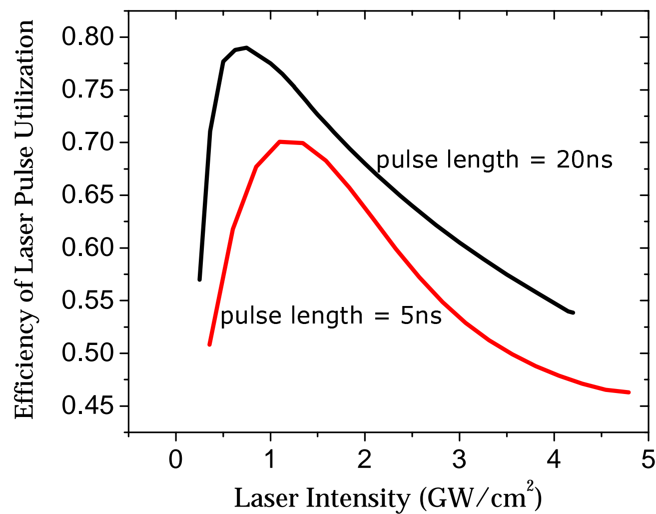

Figure 2: The calculated efficiency of laser pulse utilization vs. the laser intensity at two pulse lengths.

2.2. Laser Silicon Interaction at the Medium High Intensity Regime

In our previous treatment of laser silicon interaction at low light intensity, the absorption of the incident beam by vapor is assumed to be insignificant. This assumption is valid only for low to moderate light intensities[9]. At higher laser irradiance, the laser beam evaporates the target at the early part of the pulse; the vapor plume is then subsequently ionized by the later part of the laser pulse through the inverse Bremsstrahlung process or through the multi-photon ionization process[30]. The growth of the free electron and ion population in the vapor plume forms a plasma layer above the surface, which causes the vapor to be non-transparent to the incident laser beam, and effectively keeps the laser energy from penetrating into the ablating materials beneath. Due to this plasma shielding effect, the laser silicon ablation speed will slow down and saturate as laser intensity increases.

In our modeling, we calculate the vapor plasma properties, e.g. the electron and ions population in the plasma, and the reflectivity and absorption of the plasma to the incident beam, etc. based on the rate equation[15],

$$\frac{dn}{dt} = \gamma_i n + W_m n_0 - D\nabla^2 n - \frac{n}{\tau_R} \qquad \text{(Eq.-6)}$$

The first two terms on the right hand side of (Eq. -7), the inverse Bremsstrahlung process $\gamma_i n$ and the multi-photon ionization $W_m \times n_0$, are the growth factors for the electron and ion populations; the last two terms are the loss factors, including the deionization through diffusion $D\nabla^2 n$ and recombination n/τ_R. γ_i is the collision (or inverse Bremsstrahlung) ionization coefficient, it is given by the ratio between the energy gaining rate of electrons from the laser field and the ionization potential,

$$\gamma_i = \frac{\dfrac{eE_0{}^2\gamma_m}{2m_e(\omega_0{}^2 + \gamma_m{}^2)}}{E_{ion}} \qquad \text{(Eq.-7)}$$

Here, γ_m is the collision frequency, $\gamma_m \sim 10^{15}$/s; E_0 is the electric field strength; ω_0 is the laser field frequency, m_e is the electron mass and E_{ion} is the ionization energy. For multi-photon ionization, assume m numbers of photons are to be absorbed simultaneously to ionize the vapor, m = integer part of ($E_{ion}/h\omega_0+1$), W_m is then given as[15],

$$W_m = \left(\frac{\sigma}{\hbar\omega_0{}^2}\right)^m \times (I \times (1 - R'))^m \times \frac{\omega_0}{(m-1)!} \qquad \text{(Eq.-8)}$$

σ is the absorption cross section, $\sigma \sim 10^{-16}$ cm^2 [15] and n_0 in (Eq.-7) is the vapor density. From our vapor plume calculations, $n_0 \sim 10^{22}/cm^3$. I is the laser intensity and R' is the plasma surface reflectivity. D in (Eq.-7) is the ambipolar diffusion coefficient, and τ_R is the lifetime of electrons and ions in the plasma[16];

$$\tau_R = 5.85 \times 10^7 \times T_e{}^{4.5} / n^2$$
$$D = \frac{kT}{e} \times \frac{e}{m_e \gamma_m} \qquad \text{(Eq.-9)}$$

T is the vapor temperature, T ~ T(0)[8]. T_e is the electron temperature, T_e (K) $\sim 2.98 \times 10^4 A^{1/8} Z^{3/4} (Z+1)^{-5/8} (I\lambda\sqrt{\tau})^{1/2}$, A is the atomic number and Z is the average ionization charge[16].

In our theoretical treatment of the plasma effects on laser silicon ablation, the plasma dielectric properties are calculated using the Drude Model[17]. The time dependent plasma parameters, e.g. the population density n, the absorption coefficient α_P, and the surface reflectivity R', etc. are obtained by substituting the results from solving (Eq.-6) to (Eq.-9) into the Drude Model. In a one-dimensional approximation, where the geometry of the plasma is considered as planar, we define the transmission factor TS_v of the vapor plasma to the incident laser beam as the integration of the plasma absorption coefficient over the thickness of the absorption layer;

$$TS_v(t) = (1 - R') \times \exp[-\int_0^{x_I} \alpha_P(t, \zeta) d\zeta] \quad \text{(Eq.-10)}$$

Here x_I[16] is the thickness of the thin high pressure plasma layer where most absorption occurs. In a steady-state planar ablative flow model[31], it is defined as the layer between the expanded plasma and the ablating material.

The interaction of laser energy with silicon evaporates the target, generating a vapor plume and vapor plasma; in addition, the strong laser field also creates high density electron and hole pairs on the surface and in the bulk of the target. As a result, the absorption of laser energy is then further modified. Also, thermal and photon initiated free electron emission from the electron-hole plasma, together with the multi-photon ionization are the sources for providing the "seeds" in vapor plasma growth. The dynamics of the electron-hole plasma is characterized by the rate equation[32];

$$\frac{\partial n_{ph}}{\partial t} = D_{ph} \frac{\partial n_{ph}(z,t)}{\partial z^2} - \frac{n_{ph}(z,t)}{\tau_b} + TS_v \times (1 - R_s) \frac{I}{\hbar\omega_0} \alpha' e^{-\alpha' z} \quad \text{(Eq.-11)}$$

n_{ph} is the electron-hole density, D_{ph} is the ambipolar diffusion coefficient[33], and τ_b is the Auger recombination rate [34]. R_s and α' are determined by the plasma dielectric functions[34], with the reduced effective mass for electrons and holes taken as $m^* \sim 0.2m_e$[35,36].

Due to the continuous modification of the incident light by the vapor plasma and the electron-hole plasma during the pulse, the steady-state approximation of surface evaporation is no longer valid. Assuming again that the laser spot size is much larger than the heat affected zone, the heat conduction and evaporation front propagation are described by the one dimensional heat transport equation,

$$C\rho \frac{\partial T}{\partial t} = \nabla(\kappa \nabla T) + TS_v(t) \times (1 - R_s(t)) \times \alpha'(t) I e^{-\alpha'(t) z}$$
$$\kappa \partial T / \partial z |_{z=0} = \rho V_s H_v \quad \text{(Eq.-12)}$$

In our computational modeling, the movement of the gas-liquid interface is assumed to take place instantly once the required temperature and latent heat are reached; and the evaporation front moving speed V_s is calculated by the ratio between the steps that the gas-liquid interface advances and the time taken for the movement. The degree of condensation of the vapor plume[8] is taken into account when we compute the silicon removal speed.

A Quantum Ray DCR, ND: YAG laser system is used to provide the ablation beam in our experiments. The laser has a wavelength of 355nm, a pulse length of 5ns and a fixed repetition rate of 10 Hz. The laser beam is focused by UV lens systems; focus and spot size are determined by the knife-edge test.

Figure 3 shows both theoretical estimations and experimental measurements of laser silicon ablation speed under 5ns, 355nm laser pulses. Figure 3a is the calculated vapor plasma transmission factor TS_v given by (Eq.-10) at the end of the laser pulse. Figure 3b shows the silicon removal speed, where the theoretical estimation taking into account the plasma effects is represented by solid lines; the theoretical estimation without considering the plasma effect by dashed lines; and the experimental data by hollow circles. As indicated from the plots and from our calculation results, for laser intensities below 4 GW/cm^2, the effects of the plasma on ablation speed are rather insignificant. The ablation speed increases with laser intensity at the beginning and from ~ 4GW/cm^2 to ~ 10GW/cm^2. The ablation speed slows down and saturates beyond ~ 10GW/cm^2, where at 10GW/cm^2 the transmitted laser energy through the vapor plume is about 85% of the total energy. For 5ns laser pulses, as revealed by Figure 3b, a noticeable difference of the silicon removal speed for the cases with and without the plasma effects starts around 8GW/cm^2. We carry out the same calculations using laser pulses with a pulse length of 20ns; we find that a similar deviation starts around 3.5GW/cm^2 and saturation of the ablation speed at around 4.5GW/cm^2. We compare the calculation results with experimental data and find good consistencies.

For laser silicon ablation using nanosecond pulses working in the medium high intensity regime, where plasma shielding effects dominate, as laser intensity keeps increasing, the efficiency of laser pulse utilization keeps decreasing, and the morphologies and the quality of laser ablation generated features become more degraded. For 5ns laser pulses, when laser intensity increases above 14 GW/cm^2, fractures start to appear at the ablation crater peripheries and bottom due to stresses caused by high local thermal gradients and the great shock wave pressure.

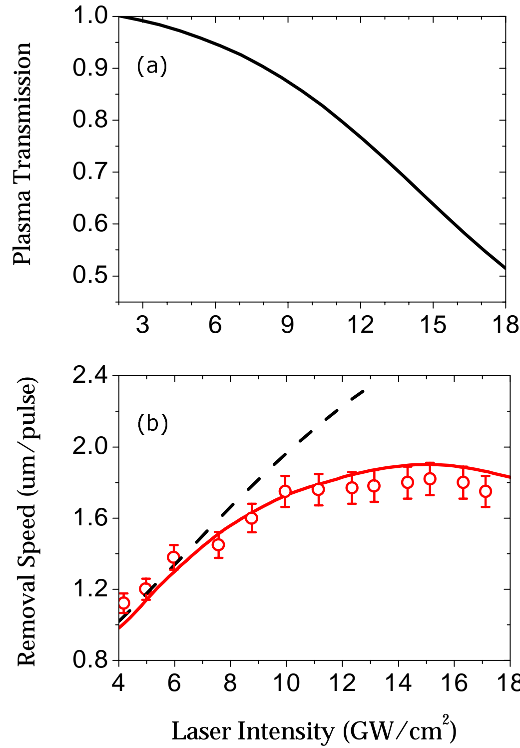

Figure3: Experimental measurements and theoretical estimations of ablation depth/pulse for 355nm, 5ns pulse: (a) the transmission factor of the vapor plasma; (b) comparison of experimental measurements (hollow circles) and theoretical estimations (with plasma, solid line; without plasma, dashed line).

2.3. Laser Silicon Interaction at the High Intensity Regime

As we further increase the laser intensities above 20 GW/cm^2 and into several hundreds of GW/cm^2 using a 5ns laser pulse, we discover that starting from around 20 GW/cm^2, the ablation speed increases again with the laser intensity. This increase in ablation speed is accompanied by violent ejection of removed materials from the ablation site.

Experimental studies of nanosecond laser ablation using 3ns, 266nm laser pulses on silicon[18, 19] and 200ns, 2.9um laser pulses on water[20] at high laser irradiances indicate a similar strong explosion behavior of the ablating materials. The major mass removal are found to take place a long time after the laser pulse and the ejection of materials lasts on a time scale much longer than the laser pulse length.

From our previous plasma calculations and discussions, we show that the plasma becomes the major source for laser energy absorption. As we further increase the laser energy, our calculations confirm that the vapor plasma will further decouple the incident laser energy from penetrating into the ablating material. Meanwhile, at high laser irradiances, the energy absorbed by the vapor plasma increases with laser intensity and becomes non-negligible. We therefore believe that in the high laser irradiance regime, the laser heated hot vapor plasma attains enough energy during the laser pulse to redistribute the incident energy through re-radiation after the laser pulse. We treat the plasma as a secondary heating source, which presumes the continued energy exchange with the ablating material after the laser pulse and considerably accelerates the ablation process. The delayed ejection phenomenon seems to support our proposed explanation.

Figure 4 shows the comparison of the ablation morphologies using 5ns pulses at 16 GW/cm^2 (left) and 125GW/cm^2 (right). The inserted figures are the comparison of the size of the ejected particulates collected during the course of our experiment near the ablation site. From Figure 4a, one can see that at 16 GW/cm^2, the laser silicon ablation undergoes the normal melting, vaporization and resolidifying processes, and the surface is sputtered by the resolidified melt. From Figure 4b, it appears that at 125GW/cm^2, silicon is removed by explosive ejections, and the surface is spallated by the great shock wave pressure loading. The inserted figures show that the sizes of ejected particulates are considerably larger at 125GW/cm^2, indicating a violent, unstable, and explosive removal of silicon.

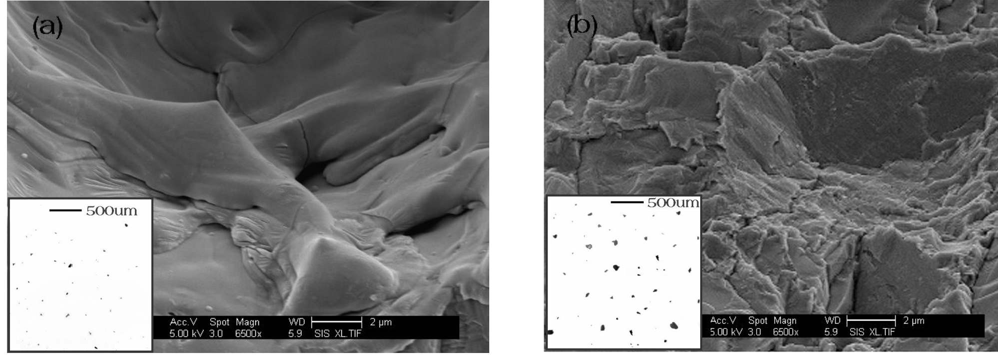

Figure 4: Comparison of the morphologies of ablation generated craters using 355nm, 5ns pulses; (a) left, at 16 GW/cm^2; (b) right, at 125 GW/cm^2. (The inserted figures are the ablation ejected particulates collected near the ablation site at these intensities).

Mechanisms for this explosive ejection at a very high heating rate could be established by considering the explosion of a metastable liquid. At the high laser irradiance regime, the short heating time and the great shock wave pressure allow the ablating system to enter deeply into the metastable state, or even beyond the critical point T_c[21]. The evaporation from the melted surface is rather weak and the primary mechanism for material removal is through the phase explosion of the metastable liquid. Assuming that the explosion occurs adiabatically, the explosive transition of metastable liquid into a mixture of liquid and vapor phase is enabled by the extra free energy Q stored in the metastable liquid. The relationship between Q and the thickness δ_e of material ejected by the phase explosion is given by[21],

$$\delta_e = \frac{Q}{\kappa_s H_v} \qquad \text{(Eq.-13)}$$

Here κ_s is the fraction of the liquid converted into vapor during the phase explosion and H_v is the latent heat for vaporization; $\kappa_s \sim 0.4$ for Aluminum[21]. Since Al is the closest element to Silicon on the periodic table and they both have the similar density, heat capacity and latent heat, we'll use $\kappa_s \sim 0.4$ for silicon estimations.

The energy that the vapor plasma attained during the laser pulse is calculated using the plasma property equations in (Eq.-6) to (Eq.-9), where the electron energy ε_e is given by[38],

$$\varepsilon_e = \frac{3}{2} n_e \times k_B T_e + n_e \times E_{ion} \qquad \text{(Eq.-14)}$$

The energy accumulated in the plasma during the laser pulse equals the free energy Q stored in the metastable liquid and is an integration of electron energy over the thickness of the plasma layer,

$$Q = \int_0^{x_I} \varepsilon_e dz \qquad \text{(Eq.-15)}$$

The energy of ions[36] is neglected in calculating Q, since ions have lower densities and much lower temperatures compared to electrons. Using (Eq.-13) to (Eq.-15) and (Eq.-12), the average ablation depth of the explosive removal and the reduced evaporation is calculated under 5ns, 355nm laser pulses. Figure 5 shows the results, where laser intensities vary from 20 GW/cm^2 to 150 GW/cm^2. Figure 5a is the comparison of experimental data and theoretical estimations, a hollow circle represents experimental measurements and the solid line represents the theoretical estimations. Shown in Figure 5b and Figure 5c, are the ablation crater profiles at 14 GW/cm^2 (left) and at 135GW/cm^2 (right).

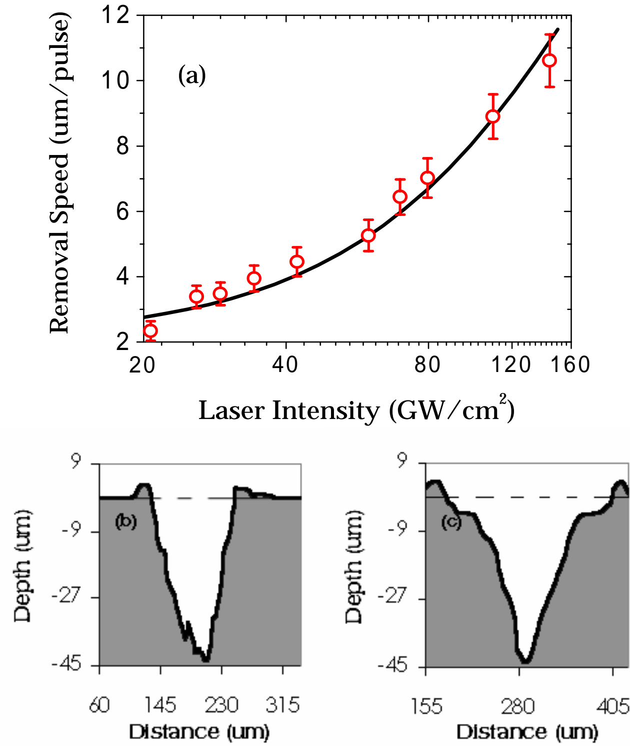

Figure5: Silicon ablation depth per pulse at high laser power for 355nm, 5ns pulses; (a) comparison of theoretical estimations (solid line) and experimental data (hollow circle); (b) the ablation crater profile at 14 GW/cm^2; (c) the ablation crater profile at 135 GW/cm^2.

The ablation depth given in Figure 5 is the averaged depth of the ablation generated crater divided by the number of applied pulses; it represents the speed that laser pulses penetrate into the target bulk and remove material from there. Another quantity often used to characterize the speed of laser matter interaction is the average removal volume; it is the volume of the crater divided by the number of applied pulses. For laser ablation at low to medium high intensities,

$$\text{average ablation depth} \approx \frac{\text{average removal volume}}{\text{laser spot area}} \qquad \text{(Eq.-16)}$$

However, at a laser intensity well beyond the medium high region, the average removal volume increases faster than the average ablation depth, and (Eq.-16) is no longer valid. As an example, shown in Figure 5b and 5c, are the ablation generated crater profiles at 14 GW/cm^2 and at 135GW/cm^2. The ratio between the average ablation depth calculated using (Eq.-16) and the actual averaged per pulse depth of the ablated crater is ~ 1.1 in Figure 5b and ~ 4 in Figure 5c.

The difference in the mass (volume) removal rate and the average ablation depth rate is due to the increased material ejections in the lateral directions caused by the increased plasma dimensions in the transverse direction and the strong shock wave. The strong shock wave mainly introduced by the plasma expansion can reach hundreds of kbar for a laser intensity above 100GW/cm^2 [39]. A strong shock wave is accompanied by the strong shock heating effect[16], where acoustic energy transforms into heating. The shock heating helps to further increase, especially in the lateral direction, the

material ejection speed. As shown by Figure 5b and 5c, by examining the ablation generated crater profile, the effect of the shock wave removal is clearly visible near the top of the ablation sample and in the transverse dimensions.

3. SUMMARY AND CONCLUSION

We have developed descriptions of the dynamics of different physical processes and ablation characteristics involved in nanosecond UV laser and silicon interaction with laser intensities ranging from 0.5 GW/cm^2 to 150 GW/cm^2. Good agreement was found between our physical modeling (without changing parameters through the calculations) and experimental verifications. Three distinct irradiance regimes are identified based on laser intensity. Results from theoretical expectations and experimental data show: (1) at low ablation intensity, silicon removal is characterized by surface evaporation, and the ablation speed increases with laser intensity; (2) at medium high ablation intensity, the increment of ablation speed with laser intensity slows down and saturates due to a strong plasma shielding effect; (3) at high ablation intensity, the laser ablation speed increases again beyond a certain threshold, and silicon is removed mostly in an explosive ejection format. Compared to the phase explosion at lower intensities, the explosive ejection at high intensities is much more significant and becomes the dominating factor in removing material. Energy re-radiated from laser heated hot plasma and plasma induced strong shock wave are found to be responsible for the acceleration in mass removal rate.

From our evaluations of using different nanosecond lasers for silicon micromachining, we find (1) in terms of removing the largest amount of silicon, given a certain laser power output, the laser pulse preferably is around the intensity where the best efficiency of laser pulse utilization is achieved; (2) a very high intensity laser pulse removes silicon at a considerably faster rate, but the quality is less and the dimensions of the ablation generated features is less controllable; (3) a longer pulse has a higher saturation fluence for the plasma shielding effect, better efficiency for laser pulse utilization, though results in worse ablation morphology and quality compared to shorter pulses.

REFERENCE

1. Butje R., Proc. SPIE 1225, 196, 1990
2. Kinsman G., Ph.D Thesis, York University, 1991
3. R.K.Singh and J. Narayan, Mater. Sci. Eng. B, Aug. 1989; vol.B3, no.3, p.217-30
4. P. P. Pronko, S. K. Dutta, D. Du, R.K. Singh, J. Appl. Phys. 78(10), November 1995, 6233-6240
5. R.K.Singh, D.R. Gilbert, J. Viatella, Mater. Sci. Eng. B, Solid-State Mater. Adv. Technol., Aug. 1996; vol.B40, no.1, p.89-95
6. Viatella, J., Singh, R.K., Thakur, R.P.S., Amorphous Silicon Technology - 1994. Symposium, 4-8 April 1994, San Francisco, CA, USA, p. 61-6
7. A. Miotello and R. Kelly, Appl. Phys. Lett. 67 (24), 1995, 3535-3537
8. Anisimov, S. I., Khokhlov, V. A., Instabilities in Laser-Matter Interaction, Boca Raton, Fla. : CRC Press, c1995, chap.3
9. Anisimov, S.I., Soviet Physics JETP, Vol. 27, no.1, July 1968, 182
10. Y. F. Lu, M. H. Hong, T. S. Low, J. Appl. Phys., vol. 85, no.5, 2899-903
11. J. Ihlemann, A. Scholl, H. Schmidt, and B. Wolff-Rottke, Appl. Phys. A: Mater. Sci. Process. 60, 411-417, (1995)
12. P. Clarke, P. E. Dyer, P. H. Key, H. V. Snelling, Appl. Phys. A. 69 (suppl.), S117-S120
13. H. Horisawa, M. Tamura, and S. Kimura, SPIE vol. 4088, P.280
14. H. C. Liu, X. L. Mao. J. H. Yoo and R.E. Russo, Appl. Phys. Lett. 75(9), 1216-1218, (1999)
15. Grey Morgan, Pep. Prog. Phys., 38, 1975, 621-665
16. Vertes, A., Gijbels, R., and Adams, F., Laser Ionization Mass Analysis, New York: Wiley & Sons, c1993, chap 4, p. 369- 431
17. Ginzburg, V.L., Propagation of electromagnetic waves in plasma, New York, Gordon and Breach [1962, c1961]
18. J. H. Yoo, S. H. Jeong, X. L. Mao, R. Greif and R. E. Russo, Appl. Phys. Lett, 76 (6), 783-785 (2000)
19. J. H. Yoo, S. H. Jeong, X. L. Mao, R. Greif, R. E. Russo, J. Appl. Phys., 88(3), 1638-1649 (2000)
20. S. L. Jacques, G. Gofstein, "Laser-flash photographic studies of Er:YAG laser ablation of water", SPIE vol. 1525, (1991), 309-312
21. M.M. Martynyuk, Zh. Tekh. Fiz., 44, 1262-1270, June 1974

22. W. W. duley, UV Lasers: effects and applications in material science, Cambridge ; New York : Cambridge University Press, 1996, chap 4
23. G. Callies, P. Berger and H. Hugel, J. Phys. D: Appl. Phys. 28, 794-806, 1995
24. Tamm, I.E., Proc. of P.N. Lebedev Physics Institute, Vol. 29, 1967, p. 231
25. Mott-Smith, H. M., Phys. Rev., 82, 885, 1951
26. D'Anna, E.; Luby, S.; Luches, A.; Majkova, E.; Martino, M., Appl. Phys. A, May 1993; vol.A56, no.5, p.429-3
27. R.C. Weast, D. Lide, “CRC handbook of chemistry and physics”, Chemical Rubber Company Press, Cleveland, 1978
28. V. N. Tokarev and A. F. H. Kaplan, J. Phys. D: Appl. Phys, 32, 1999, 1526-1538
29. R.K.Singh, D. Bhattacharya, and J. Narayan, Appl. Phys. Lett., 57, 2022 (1990)
30. Delone, N.B. and Fedorv, M. V., 1989, Usp. Fiz. Nauk., 158, 215
31. W. M. Manheimer and D. G. Colombant, Phys. Fluids, 25 (9), September 1982, 1644-1652
32. M. Morin, M. Koyanagi and M. Hirose, Jpn. J. Appl. Phys., 32 (1993), L816-819
33. A. P. Silard and M. J. Duta, Int. J. Electronics, vol. 63, no. 5, (1987), 723-731
34. M. Combescot and J. Bok, J. Luminescence, 30 (1985), 1-17
35. T. Y. Choi and C. P. Grigoropoulos, J. Appl. Phys., vol. 92, no. 9, (2002), 4918-4925
36. C. V. Shank and M. C. Downer, Mat. Res. Soc. Symp. Proc., Vol. 51 (1985), p.15-23
37. H. Howard, A.J Conneely, G.N. O'Connor, T. J. Glynn, SPIE 4876, 541(2003)
38. X. Mao, R. E. Russo, Appl. Phys. A., 64, 1-6 (1997)
39. Phipps, C. R., Turner, T. P., Harrison, R. F., York, G. W., Osborne, W. Z., Anderson, G. K., Corlis, X. F., Haynes, L. C., Steele, H. S., and Spicochi, K. C., J. Appl. Phys. 64 (3), 1 August 1988, 1083 - 1096